Electrohydrodynamic NanoDrip Printing of High Aspect Ratio Metal Grid Transparent Electrodes

*Julian Schneider, Patrik Rohner, Deepankur Thureja, Martin Schmid, Patrick Galliker, and Dimos Poulikakos**

The transparent conducting electrode is an essential component in many contemporary and future devices, ranging from displays to solar cells. Fabricating transparent electrodes requires a balancing act between sufficient electrical conductivity and high light transmittance, both affected by the involved materials, fabrication methodology, and design. While metal films possess the highest conductivity at room temperature, a decent optical transmittance can only be achieved with ultrathin films. Structuring the metal into optically invisible nanowires has been shown to be promising to complement or even substitute transparent conductive oxides as dominant transparent electrode material. Here the out-of-plane fabrication capability of the recently developed method of electrohydrodynamic NanoDrip printing to pattern gold and silver nanogrids with line widths from 80 to 500 nm is demonstrated. This fully additive process enables the printing of high aspect ratio nanowalls and by that significantly improves the electrical performance, while maintaining the optical transmittance at a high level. Metal grid transparent electrodes optimized for low sheet resistances (8 Ω sq^{-1} at a relative transmittance of 94%) as well as optimized for high transmittance (97% at a sheet resistance of 20 Ω sq^{-1}) are reported, which can be tailored on demand for the use in various applications.

1. Introduction

Transparent conducting oxides (TCOs) have been investigated as materials for transparent conducting electrodes (TCEs) for more than a century now.[1] The combination of band-gaps greater than 3 eV and carrier concentrations up to 10^{21} cm^{-3} makes them both highly transparent in the visible spectrum and electrically conductive.[2,3] The tin doped indium oxide (ITO) film is the most widely used TCO and the state-of-the-art TCE in displays, touchscreens, light emitting diodes, thin film solar cells, and smart windows.[4] The main disadvantage of ITO is its limited optical performance at very low sheet resistances. Moreover, the brittleness of the ceramic ITO films can present a bottleneck in the fabrication of highly flexible devices.[5] These disadvantages have motivated recent research efforts toward alternative material systems such as carbon nanotube[6] or silver nanowire (AgNW) networks,[7,8] metallized electrospun nanowires,[9,10] graphene layers,[11] ultrathin metal films,[12] self-forming[13] or patterned metal grids.[14–20]

Ideally, besides having very good electrical and optical performance, the new system should be low cost, flexible and include direct patterning. The former two can be achieved by the additive solution-processing of silver nanowire networks that show remarkable flexibility.[8] Depending on the application, this method however requires a post deposition structuring step. Direct patterning can be implemented with metal-wire grid electrodes when considering suitable printing technologies. While grids have been realized with nanoscale lines in several studies, the fabrication relied on subtractive multistep patterning methods such as imprinting,[14,15,20] lithography,[15] or evaporative self-assembly.[16] For microscale line widths, although not completely additive, an elegant method using selective laser sintering of a silver or nickel nanoparticle film has been presented by Hong et al.[17] and Lee et al.,[18] respectively. A direct ink writing approach of concentrated silver inks has been shown by Ahn et al., demonstrating linewidths around 5 µm.[19] TCE of very high performance have been demonstrated by electrospinning of polymer nanowires followed by the metal evaporation resulting in nanotrough networks of various metals.[9] A similar procedure was used to fabricate a network of copper wires about 1 µm in diameter that can be transferred onto a finer mesh of solution-deposited nanowires.[10] However, this interesting method is neither additive nor does it have the ability for direct patterning.

Electrohydrodynamic (EHD) printing, the technique used in this work, has been applied as a viable additive and non-contact printing technique. Conventional additive printing methods such as screen printing or inkjet printing simply lack the resolution needed for invisible metal grid TCE applications.

Dr. J. Schneider, P. Rohner, D. Thureja, M. Schmid, Dr. P. Galliker, Prof. D. Poulikakos
Laboratory of Thermodynamics in Emerging Technologies
Institute of Energy Technology
Department of Mechanical and Process Engineering
ETH Zurich
CH-8092 Zurich, Switzerland
E-mail: dpoulikakos@ethz.ch

DOI: 10.1002/adfm.201503705

Compared to ink-jet printing, high printing resolutions are achieved with EHD printing by the ejection of jets or droplets, which are much smaller than the actual nozzle size.[21,22] Yet only continuous grids with a relatively large line width above 7 µm have been demonstrated.[23–25] Visual appearance is evidently key when using metal meshes as front electrode in displays or touchscreen sensors. Metal lines of a few micrometers in width can already be disturbing for the user, necessitating patterns below the perception threshold. Moreover, the EHD printed metal meshes presented so far still make the trade-off between the electrical conductivity and optical transmittance. Thicker and hence wider lines offer higher conductivity at the expense of optical transmittance. This can be avoided by printing high aspect ratio (AR) structures.[15]

Here, we combined the 3D capabilities of EHD printing using the high-resolution NanoDrip printing mode to create thin metal walls from silver and gold colloidal inks. The basic principle and elements of the underlying physics of EHD nanodripping have been investigated in a previous study.[22] In this work, we present for the first time the printing of high-aspect ratio lines (walls) patterned into complex structures (grids), as well as a thorough electrical and optical characterization of these structures. Additionally, several key aspects concerning line integrity during printing, annealing, and potential usage are presented and the successful EHD nanoprinting of a commercial silver ink featuring low annealing temperatures and good adhesion on glass is shown for the first time.

The 80–500 nm wide and 200 nm to 1.5 µm high metal mesh lines printed here are invisible to the human eye at any observation angle and even under adverse light scattering conditions. At an aspect ratio (wall-height to wall-width) around 2–4, the electrical performance was substantially increased, while keeping the optical shadowing essentially constant. The printing principle is illustrated in **Figure 1**a. The nanowalls are built layer-by-layer through consecutive overprints, giving complete control over the aspect ratio and enabling even mixed aspect ratio lines tuned to the localized need inside a device. The grids can be printed with high resolution and accuracy as shown in the scanning electron microscopy (SEM) image in Figure 1b.

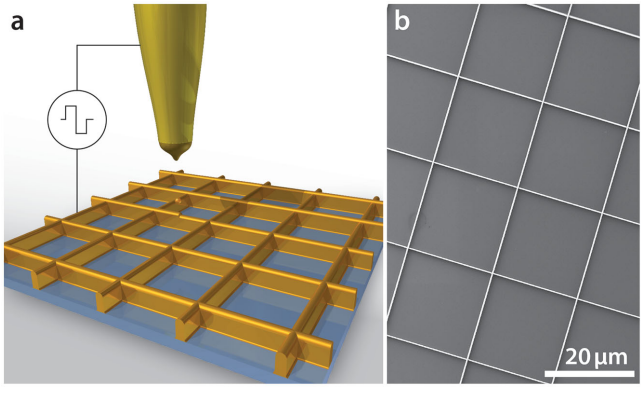

Figure 1. Illustration of high-aspect ratio patterning with electrohydrodynamic NanoDrip printing. a) The metal grids are fabricated layer-by-layer by means of overprinting. Due to nanodroplet autofocusing toward already printed out-of-plane structures and fast vaporization, the structures grow into the third dimension. b) Gold metal mesh electrode printed on glass with high aspect ratio nanowalls.

2. Results and Discussion

2.1. Concept of High Aspect-Ratio Metal Grids

The fundamental idea behind using high-aspect ratio metal grids as transparent electrode is to increase the line cross section without increasing the shadowing area. In this study, we fabricated two different type of grids, square grids and truncated hexagonal (t-hex) grids. The shadowing area can be expressed by the geometrical fill factor

$$f_F = 1 - \frac{(p-w)^2}{p^2} \tag{1}$$

for the square grid and

$$f_F = 1 - \frac{3(s_e/d)(d-w)^2 + \sqrt{3}/2 s_i^2}{3ds_e + \sqrt{3}/2 s_e^2} \tag{2}$$

for the truncated hexagonal grid with the geometrical parameters described in **Figure 2**. From the fill factor it is possible to predict the transparency T and, for a pattern size much larger and a wire size much smaller than the pitch, the sheet resistance R_s by the following equations

$$T = 1 - f_F \tag{3}$$

$$R_s = \xi \frac{\rho}{f_F} \frac{1}{h} \tag{4}$$

where ρ is the electrical resistivity of the printed material, h is the height of the lines, and ξ is a correction factor depending on printed material and lattice properties, as well as line and junction imperfections.[26] For a defined fill factor and hence transparency, an increase in the line height reduces the sheet resistance proprtional to $1/h$ (see Equation (4).

To study the effect of sparse subwavelength metal patterns in more detail and evaluate the effect of light transmittance at high incident angles, rigorous coupled wave analysis (RCWA) simulations were carried out. A 1D treatment was sufficient, as grating effects could be neglected for the sparse grids printed here. As

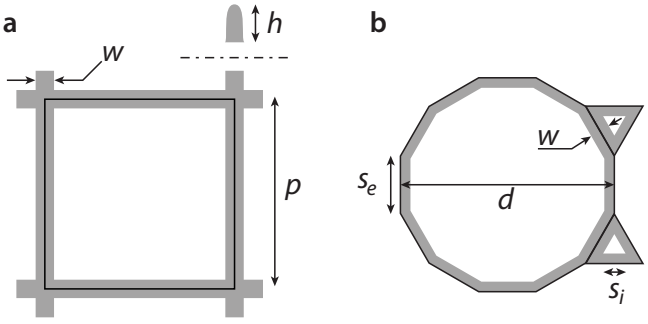

Figure 2. a) Square grid unit cell parameters. b) Truncated hexagonal (t-hex) unit cell.

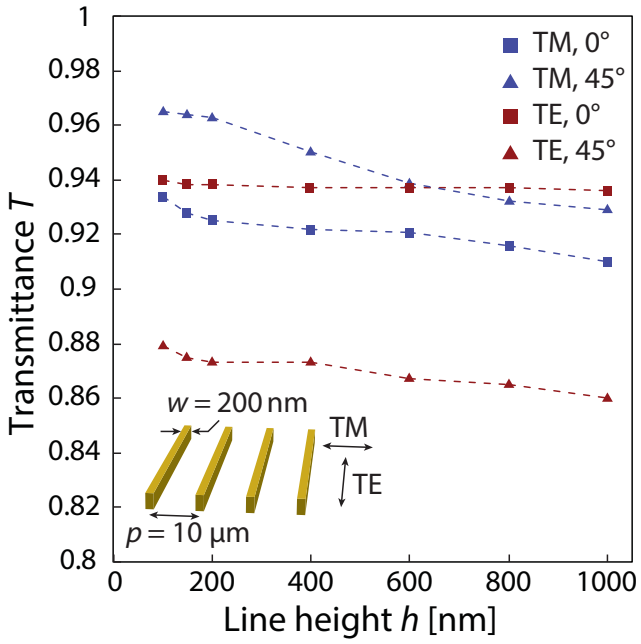

Figure 3. Rigorous coupled wave analysis of a 1D gold grid on a glass substrate. High aspect ratio lines only slightly decrease transmittance for light incidence up to 45°, while electrical performance increases by more than an order of magnitude over the shown range.

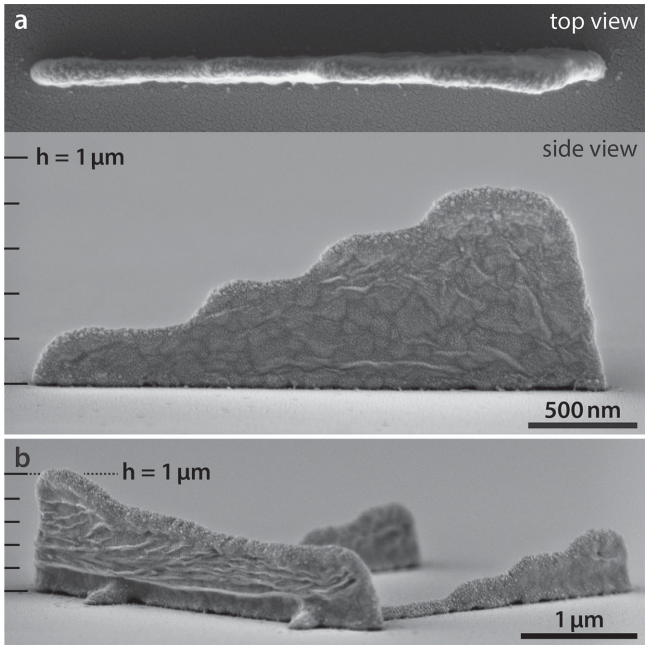

Figure 4. 3D capability demonstration of NanoDrip printing. a) Nanostairs feature imaged from the top and from the side. The number of overprints from left to right is 3, 5, 7 and 9. Width and maximal height are 120 and 870 nm, respectively, and the resulting max AR is therefore >7. b) Wider wall ($d \approx 200$ nm) printed on the left side with varying the printing speed and overlapping with two fine ($d \approx 100$ nm) nanostairs on the right. All micrographs are taken after annealing. Side views are taken at 80° tilt angle, height bars are scaled by tilt angle.

shown in **Figure 3**, the transmittance is virtually unchanged as a function of height for vertical illumination. For illumination at 45°, increasing the line aspect ratio from 0.5 to 5 decreased the transmittance of the transverse electric (TE) as well as of the transverse magnetic (TM) mode by only about 2%–3%, while electrical performance increases by an order of magnitude.

2.2. Printing and Annealing of High-Aspect Nanostructures

In EHD NanoDrip printing the ink is pulled out of a fine nozzle by a strong electric field at ejection frequencies ranging from 0.1 kHz to more than 10 kHz. The electrostatic nature of ink actuation allows the ejection of droplets more than one order of magintude smaller than the nozzle opening. In contrast to conventional inkjet printing where droplet wetting determines the final line width, fast nanoparticle migration to the substrate and efficient nanoparticle adhesion on the substrate right after impact prevents line spreading during the subsequent droplet wetting phase. With droplet sizes reaching diameters below 100 nm when printing from nozzles of about 1 µm outer diameter, nanosized structures smaller than 100 nm are readily accessible also with highly concentrated colloidal nanoparticle inks.

The nanowalls were built layer-by-layer through consecutive overprints. In previous work we have already shown that by tuning droplet ejection and vaporization time the structures will automatically grow into the third dimension as the ejected droplets are guided by electrostatic autofocusing.[22,27] In contrast to the aforementioned studies, we additionally annealed the printed structures to remove the surfactants and sinter the metal nanoparticles. **Figure 4**a shows the out-of-plane nanowall printing capability of the EHD NanoDrip printing process. While keeping the printing velocity constant and varying the number of overprints, nanostairs with a width of 120 nm were grown up to a height of 870 nm, resulting in an AR larger than 7. However, beyond demonstrating technical feasability, the AR of experimentally utilized grid electrodes was kept below 4 to make them more robust. It has to be noted that all the reported aspect ratios were measured from annealed structures. Wider lines can be readily fabricated by tuning the droplet ejection toward larger droplets or by printing two overlapping lines, as shown by the left nanowall in Figure 4b. Furthermore the robustness of the process also allowed to alter the wall height by changing the printing velocity while keeping the number of overprints constant. This illustrates the unique design flexibility of the EHD NanoDrip printing technique to create high aspect ratio nanostructures.

The finest lines achieved have a width of about 80 nm (Figure S1, Supporting Information). It is important to mention here that the width of the printed lines is roughly equivalent to the diameter of the ejected droplets. This is possible since several aspects are simultaneously fulfilled. First, impact spreading of our nanoscale droplets is negligible due to their small ratio of inertial to viscous forces.[22] Second, the metal particles efficiently adhere in the impact area before the solvent spreads over the highly wettable substrate. The high wettability of the substrate is favorable to prevent liquid accumulation, enabling the out-of-plane growth of the metal nanowalls.

The need for layer-by-layer printing is shown in Figure S2a (Supporting Information). Structures already present on the

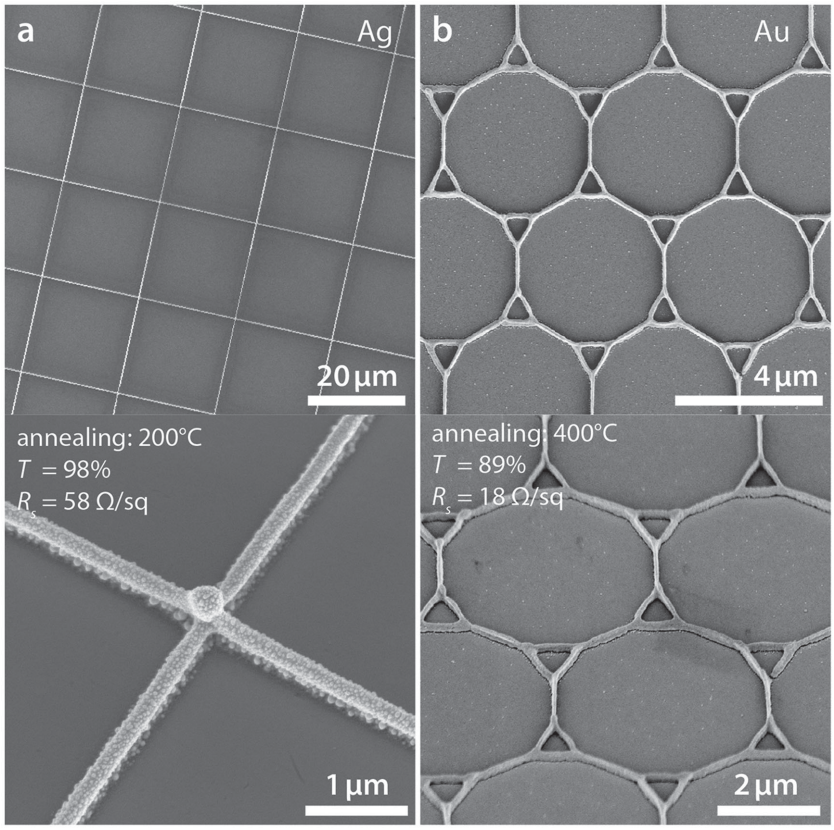

Figure 5. Printed gold and silver grids. a) Square Ag grid with a pitch of 20 µm and aspect ratio of 2.5. b) Truncated hexagonal Au grid (t-hex) with a small lattice constant of 4 µm, very fine line-width of 80 nm, and line AR of 2.3.

substrate attract the charged droplets in flight. This electrostatic autofocusing makes it difficult to reliably print next to an existing high aspect ratio structure. To mitigate this effect, the metal wall electrodes were printed layer-by-layer (Figure S2b, Supporting Information). Through further optimization of the printing velocity profile at intersections, the still apparent issue of pillar growth visible in Figure S2b (Supporting Information) could be resolved as shown in Figure S2d (Supporting Information) and **Figure 5**b.

During subsequent thermal annealing the gold nanowalls remained intact. In the case of the silver ink, disintegration of the nanowalls was often observed in the annealing process. This can be explained by the spreading of the silver nanoparticles at elevated temperatures on a film of excess surfactant present around the silver nanowall. The surfactant layer is visible in Figure 5a by the dark layer surrounding the bright silver line. By removing the surfactant layer with a short argon sputtering before annealing, the spreading and disintegration of the silver nanowalls could be avoided. The shrinkage during annealing was sometimes found to rupture high aspect ratio walls at the edge of the contacing electrode (Figure S2c, Supporting Information). Slower ramp rates during annealing and high metal loadings with a small surfactant volume fraction yielded good results.

All the optoelectronically measured samples were fabricated on glass substrates. To show the potential breadth of possible applications for our EHD NanoDrip technique, we also demonstrated the fabrication of high aspect ratio nanowalls on a flexible substrate (polyimide film). After annealing, the 25 µm thick polyimide film was imaged in an SEM while being bent at a radius of 2 mm. Figure S3 (Supporting Information) reveals that the walls show great mechanical integrity as they stay intact under bending. Their size is comparable to those fabricated on the standard glass substrates.

The adhesion of the nanowalls was investigated by a standardized scotch tape test. Even after ten pulls the silver nanowall grid remained practically intact, as can be seen in Figure S4 (Supporting Information). The minor alterations were closer examined via SEM. While the top of few nanowalls was partly harmed by the tape and the large repeated force applied with it, the base was still sticking to the substrate, proving excellent adhesion between the silver grid lines and the glass. The gold grids did not withstand the ten test cycles, as most of them were removed by the tape. The adhesion of the metal grids in general could be further improved by an adhesion layer of, e.g., polyvinylpyrrolidone if needed for a demanding application.[17]

Weak spots in the walls present sites where the walls have a higher possibility to break during sintering. They were predominantly found close to a junction point of the TCE grid. Since a junction of the truncated hexagonal grid geometry has only three legs compared to the four legs of the square grid geometry, this grids were preferred especially for very fine metal grid TCEs. Even though the figure of merit $\Phi_H = T^q / R_s$ defined by Haacke[28] is marginally lower for the t-hex grid compared to the square grid for the same line geometry and duty cycle, it is nevertheless an interesting structure in hybrid material TCEs and for organic light emitting diodes (OLED) applications, as it approximates a circular unit cell and hence potentially minimizes voltage losses in these devices.[29] A video showing an excerpt of the printing of a t-hex TCE grid including the above-mentioned optimized velocity profiles is shown in Video S1 (Supporting Information).

2.3. Electrical and Optical Performance of Printed Grids

To remove the insulating surfactant around the nanoparticles and induce the sintering process, the printed structures were thermally annealed. In order to render as-printed gold grids electrically conductive, a minimal annealing temperature of 250 °C was required. In contrast, silver inks obtained excellent conductivity already at 150 °C (**Figure 6**a). These low temperatures make the printed silver and gold grids compatible with flexible polymer substrates such as polyethylene terephthalate (PET) and polyimide films, respectively. The influence of the

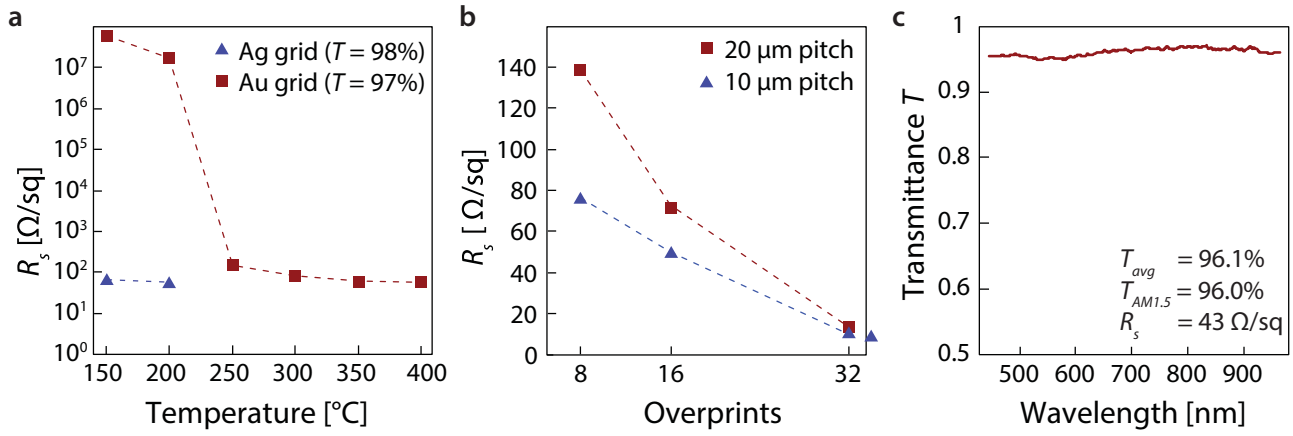

Figure 6. Annealing and optoelectronic performance of printed grids. a) Sheet resistance as a function of annealing temperature. Gold grids are virtually nonconductive before annealing. Minimally 250 °C is required to remove the surfactant layer and sinter the gold nanoparticles. The silver is already fully sintered at 200 °C. b) The sheet resistance decreases with overprints while transmittance remains virtually unaltered. c) Transmittance spectrum of a gold grid with 20 µm pitch.

number of overprints on the electrical performance is shown in Figure 6b. The sheet resistance decreases with increasing overprints (line heights) while transmittance remains virtually unchanged, in accordance with Equation (4).

Optical transmittance measurements in this study were normalized to the underlying glass substrate. The transmittance was found to be independent of the wavelength in the range of visible light for both Au and Ag grids. The transmittance spectrum of a gold grid with a pitch of 20 µm and with an intermediate AR of about 1.5 is shown in Figure 6c. Generally, the results were in very good agreement with the transmittance estimations made by simple geometrical shadowing calculations (Equation (3)), never deviating more than 0.5%. Due to the experimental difficulty of optically characterizing the small area grids, no measurements at high incident angles were carried out to backup the good results from the RCWA simulation. However, Kuang et al. have shown very good optical properties for their metal nanowall gratings for periods larger than the optical wavelength.[15] They have also shown that this performance could additionally be improved for high angles of incident light by encapsulating the grids inside a polymer film.[30]

The electrical and optical performance of our grids are summarized in the R_s-T plot shown in **Figure 7**. We have selected some of the best-performing recently published TCEs by various fabrication techniques as well as other EHD printed electrodes and ITO as references. Comparing our results to the coarser EHD printed silver grids by Jang et al.[23] and Park and Hwang[24] our gold grids show higher transmittance at the same sheet resistance while being more than one order of magnitude finer. Unlike solution-processed silver nanowire or carbon nanotube TCEs, our grids do not have a percolation threshold and hence are advantageous at low coverages. Indeed Figure 7 shows that with our EHD NanoDrip printing technique relative transmittances as high as 97% can be reached (at 20 Ω sq^{-1}), being superior to the silver nanowire or carbon nanotube networks[31] in the high transmittance regime. Another promising technique that successfully adresses this issue uses metal evaporation on electrospun polymer wires to achieve exceptional optoelectronic performance due to highly uniform networks of very long polymer fibers.[9,10] Compared to this technique our fully additive approach does not waste any material, allowing the efficient use of oxidation resistant noble metals such as gold or silver. To the best of our knowledge our high aspect ratio nanogrids show the best performance reported in the class of additively fabricated transparent conducting electrodes.

For the square grids, the width of the nanowalls was varied from 100 to 500 nm, whereas the line width was kept constant at 80 nm for all t-hex grids. As expected, the lowest sheet resistance of 8 Ω sq^{-1} at 94% transmittance was found for the sample with 500 nm wide and 1.5 µm high walls (Figure 7 and Figure S5, Supporting Information). Simultaneously increasing pitch and width improves the R_s-T performance when keeping the aspect ratio constant as the cross-sectional area scales with w^2. The larger pitch however will have adverse effects on the ohmic loss in optoelectronic devices because the off-grid electron transport distances become longer. Thus, depending on the needs of the application, either fine and dense grids or sparse grids with wider walls are preferred. A significant advantage of the flexibility of NanoDrip printing is that our TCEs can be perfectly tailored to the requirements of a specific device. Additionally they can be combined with other novel TCE materials such as conductive polymers or graphene to reduce roughness or improve local charge collection.

A controlled roughness is generally important for thin film devices such as thin film photovoltaics (TFPV) and OLED, as it changes light scattering properties and affects step coverage during the conformal deposition of the active emitter/absorber material.[32] This is inherent to all metal grid-based TCEs but has to be especially considered for high aspect ratio structures. EHD printed nanowalls are rounded at the top and also around the base, largely mitigating the problem of defective conformal coating. The cross-section of the lines could be further optimized to reduce the risk of defects during (conformal) thin film deposition. Moreover, EHD nanodripping or spraying could be used to directly pattern the emitter material or to deposit a smoothing layer in-between the grids consisting of, e.g., a conductive polymer such as

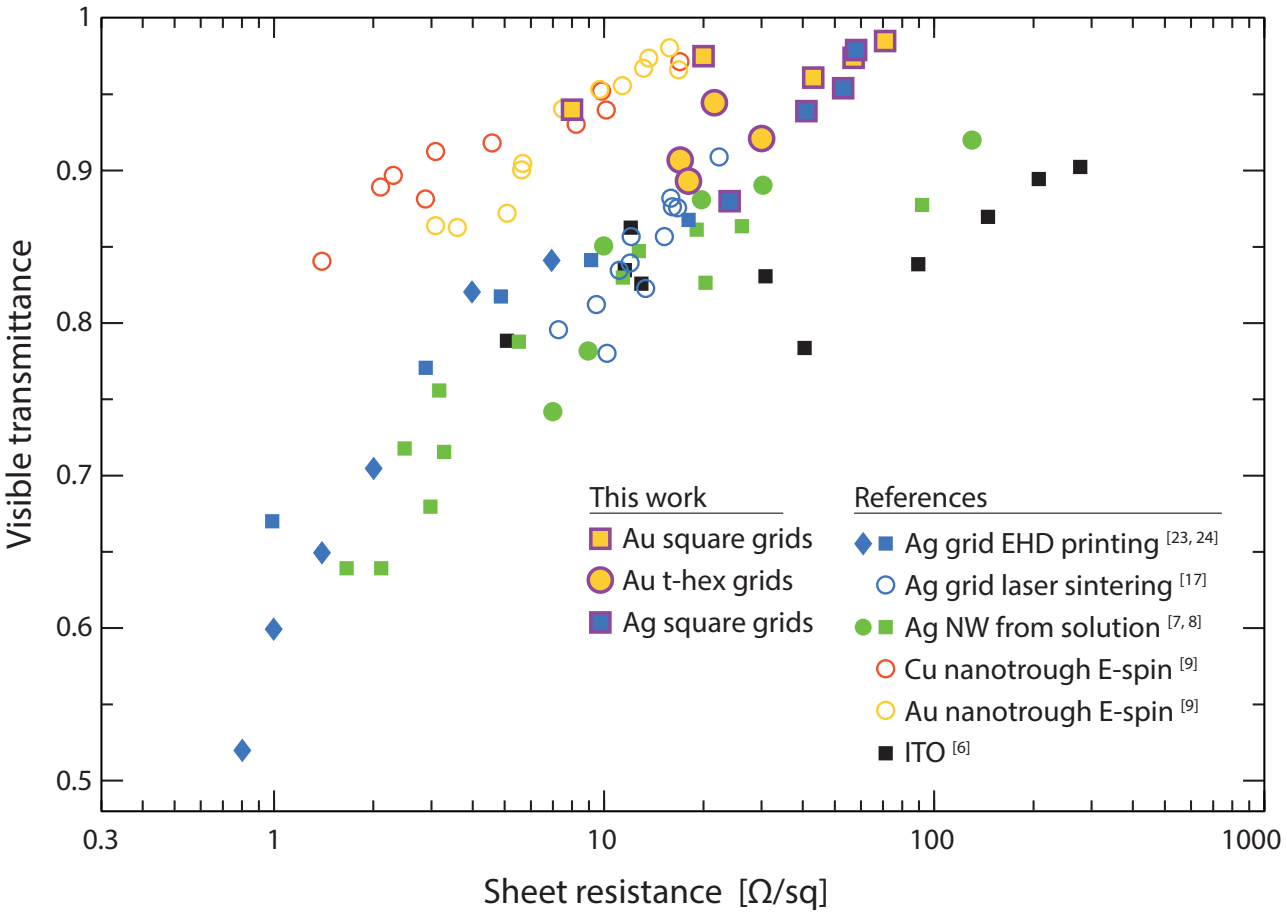

Figure 7. Sheet resistance versus visible transmittance (without substrate) for the printed gold and silver grids compared to the state-of-the-art research materials and methods. The chosen references show the performance of TCE fabricated by EHD printing[23,24] by metal deposition on electrospun polymer fiber networks,[9] by drop-casted silver nanowire solutions,[7,8] or by laser sintered colloidal inks.[17] ITO films[6] (noncommercial) are plotted as an additional reference. Electrodes fabricated by material-intensive subtractive techniques are plotted with empty symbols.

poly(3,4-ethylenedioxythiophene)-poly(styrenesulfonate) (PEDOT:PSS).

If employed as TCEs in thin film solar cells, the presented high aspect ratio grids could decrease the area loss while keeping the resistance loss constant. To further increase the overall efficiency, a variety of plasmonic structures have been proposed to trap the light in the semiconductor thin film.[33,34] Pala et al. for example have investigated nonperiodic arrangements of nanoscale metal lines for the realization of very effective broadband light-trapping layers.[35] As a proof of concept, similar periodic and nonperiodic line gratings with a pitch of 500 nm have been readily fabricated by NanoDrip printing (Figure S6, Supporting Information).

A major challenge that remains to be solved is the low printing speed of the reported structures. The patterning of 100 µm × 100 µm takes almost half an hour for sparse grids. To increase the patterning speed, two approaches have to be implemented. First, the printing process from a single nozzle has to be accelerated by using inks with high metal nanoparticle loadings printed at increased droplet ejection frequencies. Second, the massive parallelization of printing nozzles is necessary to pattern high aspect ratio metal grids with NanoDrip printing on commercial scales. This involved task could be achieved in the future by implementing dense nozzle arrays on large area silicon-based printheads fabricated by standard semiconductor device manufacturing technology. Additional to the speed-up of the deposition process, further investigations on the mechanical (bending) properties on flexible substrates, adhesion as well as haze and clarity performance remain the central topics of future work.

3. Conclusion

We have combined the nanoscale resolution and the 3D capabilities of electrohydrodynamic NanoDrip printing to pattern high aspect ratio silver and gold metal grid electrodes. With an aspect ratio of 3, the electrical performance could be increased without increasing optical shadowing. The overall optoelectronic performance exceeds conventional ITO materials and is comparable to the best materials reported. The fully additive process has the potential to complement other novel TCE materials such as graphene or conductive polymers like PEDOT:PSS resulting in high performance TCEs which are more flexible and yet less expensive than today's TCOs. In contrast to lithographic patterning methods, no material is wasted, allowing the

use of oxidation resistant noble metals such as gold or silver. The nanoscale patterns can be printed on demand and engineered according to the specific needs within the device. With annealing temperatures as low as 150 °C they can be combined with flexible substrates. Due to the small line geometries, the printed electrodes are invisible to the eye and may therefore find applications where visual appearance is of utmost importance, such as touchscreens or OLED displays. The method presented here is a significant step forward, adding to the existing landscape of approaches aiming at the facile fabrication of TCEs with high performance.

4. Experimental Section

Colloidal Inks: Two different colloidal gold inks and one silver ink were used for this study. A commercial gold nanoparticle suspension from ULVAC Technologies (Au1TeH) with particle diameters between 3 and 7 nm was diluted with *n*-tetradecane to 3 wt% solid content. For the truncated hexagonal grids, a custom made ink with 5 nm gold particles capped with 1-octanethiol as stabilizing surfactant was used.[36] This ink was washed several times to remove any excess surfactant and diluted in tetradecane to optical densities similar to the ULVAC ink. A commercial silver ink from NanoMAS Technologies (NanoSilver) with nanoparticle diameters between 2 and 10 nm was diluted in *n*-tridecane to 3 wt% solid content. All inks were filtered with a 0.1 µm syringe filter one day after dilution and homogenized prior to its usage.

Substrate Preparation: Borosilicate glass wafers with a thickness of 500 µm were patterned with gold electrode pads separated by a distance of 100 µm for electrical characterization of the printed grids. The gold pads were fabricated by standard photolithography using either lift-off (LOR, MicroChem) or a gold etch patterning approach (AZ resist, Microchemicals). The chromium/gold (5 nm/35 nm) layers were deposited by e-beam evaporation (Evatec). Right before printing, the 7 mm × 7 mm glass chips were cleaned and rendered hydrophilic by an O_2 plasma ashing step or by a short dip in fresh piranha solution (3:1 volumetric mixture of H_2SO_4(conc.):H_2O_2(30%)). The polyimide substrates with a thickness of 25 µm were cleaned with ethanol and O_2 plasma treated before printing.

Printing: The electrohydrodynamic printing setup used in this study was equipped with a precision nanostage (MadCityLabs Nano-LP300) and a confocal laser microscope for in situ visual inspection and estimation of grid height.[22] The nozzles were fabricated from borosilicate capillaries (World Precision Instruments, 1 mm outer diameter). The capillaries were pulled to an outer diameter of 1–1.8 µm (Sutter Instruments P-97) and coated with a thin Ti/Au layer (10 and 100 nm) using an e-beam evaporation system (Plassys MEB550S). They were back-filled with the ink and moved to a working distance of 3–5 µm above the substrate before a square wave of 180–230V_p at 1 kHz was applied to actuate the printing process. Printing velocity was in the range of 1–10 µm s^{-1} with a standard value of 2–5 µm s^{-1} for the gold inks and 10 µm s^{-1} for the silver ink. The velocity was increased at the grid intersections in some experiments to prevent height differences and pillar growth. Primitive square grids as well as truncated hexagonal grids were printed, with unit cells and parameters shown in Figure 2.

Thermal Annealing: To remove the insulating surfactant around the nanoparticles and induce the sintering process, the printed structures were thermally annealed in a rapid thermal annealing system (Jipelec Jetfirst RTA) using temperatures from 150 to 400 °C in a vacuum environment. To investigate the optimal annealing temperature, the sample was heated at a ramp rate of 1 °C s^{-1}, held for 10 min at the target temperature and subsequently cooled passively to reach room temperature. After the electrical characterization, the grids were heated up to the next higher target temperature. Target temperatures were 150, 200, 250, 300, 350, and 400 °C for gold and 150 and 200 °C for silver. The truncated hexagonal gold grids were heated up to 400 °C directly at a rate of 1 °C s^{-1} and annealed for 30 min. The gold demonstration structures on polyimide were heated up to 250 °C at a rate of 1 °C s^{-1} and annealed for 30 min.

Adhesion Tests: The adhesion between metal grid and substrate was investigated by a standardized scotch tape test (IPC-TM-650 2.4.1E). 3M Brand 600 Scotch tape obtained from an office supply store was firmly pressed onto the grids and eventual air pockets were removed by repeatedly rubbing from one side to the other. The tape was peeled off rapidly and a new piece of tape was used to repeat the procedure while the directionality of the tape was changed every time. Ten cycles were carried out. The sample was imaged before and after with bright field microscopy using a 50× objective.

Electrical Measurements: The square metal grids with an overall grid length of 100 µm were printed to bridge the gap between two prefabricated Au electrode pads. The grid resistance, measured with a probe station connected to a Keithley 4200 source meter unit, was therefore directly translated to the sheet resistance. Collinear four-point probing on the two electrode configuration was carried out to eliminate the contact resistance between tungsten probes and Au electrode pads. The resistive losses in the contact pad itself were found to be negligible (well below 1 Ω).

Optical Characterization: An optical setup based on two microscope objectives was built to make transmittance measurements of small areas. A fiber coupled Xenon lamp was used as light source. The light was focused into the back focal plane of a Zeiss LD Plan-Neofluar 40× (NA 0.6) objective and captured after traversing the sample by a similar objective (LD Plan-Neofluar 63×, NA 0.75). Spectra of the transmitted light were recorded with a spectrometer (Princeton Instruments) in the wavelength range of 440–970 nm and normalized to a bare glass substrate by

$$T(\lambda) = 1 - \frac{I_{\text{glass}}(\lambda) - I_{\text{sample}}(\lambda)}{I_{\text{glass}}(\lambda) - I_{\text{dark}}(\lambda)} \tag{5}$$

where I_{dark} was used to correct for the dark counts of the photodiode. The spectral transmittance $T(\lambda)$ was then weighed for AM1.5 solar spectrum to derive an average transmittance $T_{\text{AM1.5}}$, calculated by

$$T_{\text{AM1.5}} = \frac{\int_{440}^{970} T(\lambda) \times I_{\text{AM1.5}}(\lambda)\,\mathrm{d}\lambda}{\int_{440}^{970} I_{\text{AM1.5}}(\lambda)\,\mathrm{d}\lambda} \tag{6}$$

Optical transmittance simulations were performed by 1D rigorous coupled wave analysis using the MATLAB code from Pavel Kwiecien (rcwa-1d). For simplicity, the cross-section of the metal wires were modeled as square shape. The values reported were extracted for a wavelength of 550 nm. The refractive index used for the borosilicate substrate was $n = 1.518$ and for the gold grid $n = 0.422 - 2.346i$, respectively.

Characterization: The geometry and morphology of the printed and thermally annealed grids were analyzed by SEM imaging (Zeiss ULTRA 55 or ULTRA plus). To reduce charging, N_2-stream charge compensation inside the SEM was used or samples were coated prior to inspection with a thin 2–5 nm Au/Pd layer using a small sputter coating system (Balzers BAL-TEC SCD-050).

Supporting Information

Supporting Information is available from the Wiley Online Library or from the author.

Acknowledgements

J.S. and P.R. contributed equally to this work. This work was supported by the Swiss National Science Foundation through grant 200021_146180. The authors want to acknowledge Patrizia Richner for fabricating the printing nozzles. Clean room work was carried out in the FIRST Center

for Micro- and Nanoscience at ETH Zurich and in the Binnig and Rohrer Nanotechnology Center at IBM Zurich Research Laboratories.

Received: September 1, 2015
Revised: October 14, 2015
Published online: December 15, 2015

[1] K. Ellmer, *Nat. Photonics* **2012**, *6*, 808.
[2] F. Matino, L. Persano, V. Arima, D. Pisignano, R. I. R. Blyth, R. Cingolani, R. Rinaldi, *Phys. Rev. B* **2005**, *72*, 085437.
[3] A. Gondorf, M. Geller, J. Weissbon, A. Lorke, M. Inhester, A. Prodi-Schwab, D. Adam, *Phys. Rev. B* **2011**, *83*, 212201.
[4] C. G. Granqvist, *Thin Solid Films* **2014**, *564*, 1.
[5] Z. Chen, B. Cotterell, W. Wang, E. Guenther, S. J. Chua, *Thin Solid Films* **2001**, *394*, 202.
[6] T. M. Barnes, M. O. Reese, J. D. Bergeson, B. A. Larsen, J. L. Blackburn, M. C. Beard, J. Bult, J. van de Lagemaat, *Adv. Energy Mater.* **2012**, *2*, 353.
[7] J. Y. Lee, S. T. Connor, Y. Cui, P. Peumans, *Nano Lett.* **2008**, *8*, 689.
[8] S. De, T. M. Higgins, P. E. Lyons, E. M. Doherty, P. N. Nirmalraj, W. J. Blau, J. J. Boland, J. N. Coleman, *ACS Nano* **2009**, *3*, 1767.
[9] H. Wu, D. S. Kong, Z. C. Ruan, P. C. Hsu, S. Wang, Z. F. Yu, T. J. Carney, L. B. Hu, S. H. Fan, Y. Cui, *Nat. Nanotechnol.* **2013**, *8*, 421.
[10] P. C. Hsu, S. Wang, H. Wu, V. K. Narasimhan, D. S. Kong, H. R. Lee, Y. Cui, *Nat. Commun.* **2013**, *4*, 2522.
[11] S. Bae, H. Kim, Y. Lee, X. F. Xu, J. S. Park, Y. Zheng, J. Balakrishnan, T. Lei, H. R. Kim, Y. I. Song, Y. J. Kim, K. S. Kim, B. Ozyilmaz, J. H. Ahn, B. H. Hong, S. Iijima, *Nat. Nanotechnol.* **2010**, *5*, 574.
[12] H. M. Stec, R. J. Williams, T. S. Jones, R. A. Hatton, *Adv. Funct. Mater.* **2011**, *21*, 1709.
[13] B. Han, K. Pei, Y. L. Huang, X. J. Zhang, Q. K. Rong, Q. G. Lin, Y. F. Guo, T. Y. Sun, C. F. Guo, D. Carnahan, M. Giersig, Y. Wang, J. W. Gao, Z. F. Ren, K. Kempa, *Adv. Mater.* **2014**, *26*, 873.
[14] M. G. Kang, L. J. Guo, *Adv. Mater.* **2007**, *19*, 1391.
[15] P. Kuang, J. M. Park, W. Leung, R. C. Mahadevapuram, K. S. Nalwa, T. G. Kim, S. Chaudhary, K. M. Ho, K. Constant, *Adv. Mater.* **2011**, *23*, 2469.
[16] J. H. Park, D. Y. Lee, Y. H. Kim, J. K. Kim, J. H. Lee, J. H. Park, T. W. Lee, J. H. Cho, *ACS Appl. Mater. Inter.* **2014**, *6*, 12380.
[17] S. Hong, J. Yeo, G. Kim, D. Kim, H. Lee, J. Kwon, H. Lee, P. Lee, S. H. Ko, *ACS Nano* **2013**, *7*, 5024.
[18] D. Lee, D. Paeng, H. K. Park, C. P. Grigoropoulos, *ACS Nano* **2014**, *8*, 9807.
[19] B. Y. Ahn, D. J. Lorang, J. A. Lewis, *Nanoscale* **2011**, *3*, 2700.
[20] M. G. Kang, H. J. Park, S. H. Ahn, L. J. Guo, *Sol. Energy Mater. Sol. Cells* **2010**, *94*, 1179.
[21] J. U. Park, M. Hardy, S. J. Kang, K. Barton, K. Adair, D. K. Mukhopadhyay, C. Y. Lee, M. S. Strano, A. G. Alleyne, J. G. Georgiadis, P. M. Ferreira, J. A. Rogers, *Nat. Mater.* **2007**, *6*, 782.
[22] P. Galliker, J. Schneider, H. Eghlidi, S. Kress, V. Sandoghdar, D. Poulikakos, *Nat. Commun.* **2012**, *3*, 890.
[23] Y. Jang, J. Kim, D. Byun, *J. Phys. D: Appl. Phys.* **2013**, *46*, 155103.
[24] J. Park, J. Hwang, *J. Phys. D: Appl. Phys.* **2014**, *47*, 405102.
[25] B. Seong, H. Yoo, V. D. Nguyen, Y. Jang, C. Ryu, D. Byun, *J. Micromech. Microeng.* **2014**, *24*, 097002.
[26] D. S. Ghosh, T. L. Chen, V. Pruneri, *Appl. Phys. Lett.* **2010**, *96*, 041109.
[27] P. Galliker, J. Schneider, D. Poulikakos, *Appl. Phys. Lett.* **2014**, *104*, 073105.
[28] G. Haacke, *J. Appl. Phys.* **1976**, *47*, 4086.
[29] K. Neyts, A. Real, M. Marescaux, S. Mladenovski, J. Beeckman, *J. Appl. Phys.* **2008**, *103*, 093113.
[30] P. Kuang, J. M. Park, G. Y. Liu, Z. Ye, W. Leung, S. Chaudhary, D. Lynch, K. M. Ho, K. Constant, *Opt. Express* **2013**, *21*, 2393.
[31] S. De, P. J. King, P. E. Lyons, U. Khan, J. N. Coleman, *ACS Nano* **2010**, *4*, 7064.
[32] L. B. Hu, H. Wu, Y. Cui, *MRS Bull.* **2011**, *36*, 760.
[33] H. A. Atwater, A. Polman, *Nat. Mater.* **2010**, *9*, 205.
[34] W. Wang, S. M. Wu, K. Reinhardt, Y. L. Lu, S. C. Chen, *Nano Lett.* **2010**, *10*, 2012.
[35] R. A. Pala, J. S. Q. Liu, E. S. Barnard, D. Askarov, E. C. Garnett, S. H. Fan, M. L. Brongersma, *Nat. Commun.* **2013**, *4*, 2095.
[36] P. Richner, H. Eghlidi, S. K. Kress, M. Schmid, D. J. Norris, D. Poulikakos, unpublished.